ELSEVIER

The Spine Journal 4 (2004) 141–152

THE SPINE JOURNAL

Human lumbar facet joint capsule strains: I. During physiological motions

Allyson Ianuzzi, MS[a], Jesse S. Little, MS[a], Jonathan B. Chiu, MS[a], Avi Baitner, MD[b], Greg Kawchuk, DC, PhD[c], Partap S. Khalsa, DC, PhD[a,*]

[a]*Department of Biomedical Engineering, HSC T18-030, Stony Brook University, Stony Brook, NY 11794-8181, USA*
[b]*Department of Orthopaedics, Stony Brook University, Stony Brook, NY 11794-8181, USA*
[c]*Faculty of Kinesiology, University of Calgary, 2500 University Drive, Calgary, Alberta T2N 1N4, Canada*

Received 3 February 2003; accepted 6 July 2003

Abstract

BACKGROUND CONTEXT: The lumbar facet joint capsule is innervated with nociceptors and mechanoreceptors, and is thought to play a role in low back pain as well as to function proprioceptively.
PURPOSE: In order to examine the facet capsule's potential proprioceptive role, relationships between intracapsular strain and relative spine position were examined.
STUDY DESIGN/SETTING: Lumbar facet joint capsule strains were measured in human cadaveric specimens during displacement-controlled motions.
METHODS: Ligamentous lumbar spine specimens (n=7) were potted and actuated without inducing a moment at the point of application. Spines were tested during physiological motions of extension, flexion, left and right lateral bending. Intervertebral angulations (IVA) were measured using biaxial inclinometers mounted on adjacent vertebrae. Joint moments were determined from the applied load at T12 and the respective moment arms. Capsule plane strains were measured by optically tracking the displacements of infrared reflective markers glued to capsule surfaces. Statistical differences ($p<.05$) in moment, IVA and strain were assessed across facet joint levels using analysis of variance and comparison of linear regressions.
RESULTS: The developed moments and IVAs increased monotonically with increasing displacements; the relationships were highly correlated for all four motion types. Although highly variable among specimens, principal strains also increased monotonically in magnitude with increasing displacements during extension and flexion, but were more complex during lateral bending. At a given joint level, the absolute magnitudes of principal strains and IVA were largest during the same motion type.
CONCLUSIONS: Distinct patterns in principal strains and IVA were identified during physiological motions, lending biomechanical support to the theory that lumbar facet joint capsules could function proprioceptively.

Keywords: Plane strain; Lumbar spine; Facet joint capsule; Biomechanics

Introduction

The lumbar facet joint capsule can be a source of low back pain and may also serve proprioceptive functions. Whereas the former is relatively well established [1–3], the proprioceptive role of the facet capsule is largely theoretical [4]. The facet capsule is innervated by low threshold mechanoreceptors [1,5,6], similar to other peripheral joints [7,8]. The presence of low threshold, slowly and rapidly adapting mechanosensitive neurons imply that these afferents could provide information regarding joint movement and/or position [9]. In the knee [8], the neural response of capsule mechanoreceptors during motions is proportional to suprathreshold capsule tension. Hence, for facet capsule afferents to function proprioceptively during physiological motions of the spine, the capsules would have to be loaded such that their intracapsular strains would be proportional, in some fashion, to the spine's position.

FDA device/drug status: not applicable.

Support in whole or in part was received from National Institutes of Health (NIH)/National Center for Complementary and Alternative Medicine/Palmer under Grant SU01AT001701-01 and NIH/National Institute of Arthritis and Musculoskeletal and Skin Diseases under Grant 1R03AR46865. Nothing of value received from a commercial entity related to this research.

* Corresponding author. Department of Biomedical Engineering, HSC T18-030, Stony Brook University, Stony Brook, NY 11794-8181, USA. Tel.: (631) 444-2457; fax: (631) 444-6646.
E-mail address: partap.khalsa@stonybrook.edu (P.S. Khalsa)

1529-9430/04/$ – see front matter
doi:10.1016/j.spinee.2003.07.008

Afferents innervating the facet joint capsule and the surrounding tissue in the cat [10] and rabbit [11] are responsive to direct capsule loading (ie, strains). Measuring in vivo facet capsule strains in humans with current technology is impractical and unethical, because of the invasive nature of the procedures. However, in situ strains can be measured using human cadaveric spines. During motions of flexion, extension, lateral bending or rotation, using cadaveric, intact, human lumbar spine specimens, consistent patterns of stretch were not found in the extension ratios of lumbar facet joint capsules [12]. In isolated human cervical spine motion segments (eg, C3–C4 motion segment) after flexion and extension, intracapsular principal plane strains were complex, without a clear pattern [13]. In isolated human lumbar motion segments (eg, L4–L5), increasing flexion moment produced increasing uniaxial strain of capsule ligaments [14], but these data were not from direct measurements of the capsule itself. Thus, the biomechanical data in the literature do not yet provide substantive support for the theory of facet capsules functioning proprioceptively.

The current study examined a component of this proprioceptive theory by determining whether strains of lumbar facet joint capsules, during physiological motions of flexion, extension and lateral bending, were proportional to spine motion. A displacement-controlled apparatus was constructed that could repeatedly and reliably create the desired motions. A commercial kinematic system was used to obtain optical measurements of three-dimensional (3D) displacements of small markers glued to the capsule surfaces. Intracapsular plane strains were calculated from these displacements, accounting for the movement of the capsule plane by using an extension of the method of Hoffman and Grigg [15]. Preliminary data have been previously reported in abstract and thesis form [16,17].

Methods

Spine specimens

Human lumbar spine specimens (n=7; mean age, 50 years±12.96 SD; range, 38 to 64 years; sex: 6 men, 1 woman) were shipped frozen from National Disease Research Interchange (Philadelphia, PA). Specimens (T12 to sacrum) were unembalmed and procured within 24 hours postmortem from donors without history of spine pathology. Before testing, the spines were dissected free of all superficial tissue (including insertions of multifidi muscles) to expose the facet joint capsules, thus resulting in a "ligamentous" specimen. Specimens were kept moist with periodic misting of phosphate buffered saline (PBS, pH 7.4) and wrapped in PBS-soaked gauze. A specimen was first oriented vertically by visual inspection such that the L3 and L4 endplates were parallel to the testing surface; and then the sacrum was potted in a quick-setting epoxy (Bondo, Bondo Corporation, Atlanta, GA). After dissection, or at the completion of partial testing, spines were wrapped in plastic, double-bagged, and frozen (−80C). Specimens were allowed to undergo no more than five freeze-thaw cycles, because further cycles may have compromised the tissue's biomechanical properties [18].

Loading apparatus

Physiological motions of the specimens were tested using a custom, displacement-controlled loading apparatus (Fig. 1). The linear actuator consisted of a sled moving on a precision screw, which was fitted with an antibacklash nut and coupled to a torque motor (Model 317; Galil, Inc., Rocklin, CA) and optical encoder (MX21-559; Duncan Electronics, Tustin, CA). Actuator movement was controlled by a digital, programmable, proportional, integrative and derivative (PID) controller (Model 1704; DMC, Galil, Inc., CA; resolution 0.8 μm, repeatability better than 5.0 μm). A program (LabVIEW, version 6.0; National Instruments, Inc., Austin, TX) was written for implementation of a variety of dynamic loading protocols [17].

The entire apparatus sat on a flat steel slab (78 cm×76 cm×2.5 cm). A potted specimen was locked into the slab and coupled to the actuator such that the actuator was horizontal at a given peak displacement. The coupling consisted of a rod in series with a force transducer (Model 9363-D1-50-20P1; Revere Transducers, Tustin, CA; range, ±220 N, resolution 0.02 N), which was connected to the actuator by means of a low-friction universal joint. To connect the rod to the specimen, a U-shaped collar was attached to the T12 vertebral body, creating a single degree of freedom and eliminating off-axis loading of the force transducer. Intervertebral angulation (IVA) at a given joint segment was measured using two biaxial inclinometers (Model UI113077; CFX Technologies, West Chester, PA; range±90 degrees, resolution 0.2 degrees) attached to the respective anterior vertebral bodies. All analog signals (displacement, load, four angles) were collected at 1,000 Hz by an A/D converter (Model PCI-MIO16-E1; National Instruments, Inc., TX) to synchronize collection, low-pass filtered (Model 3905B

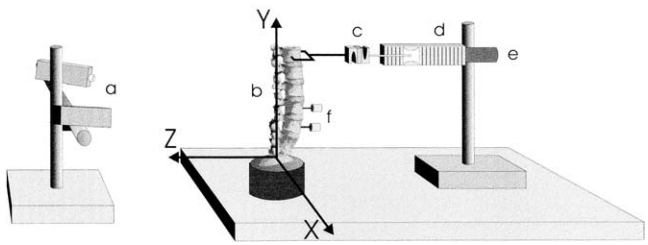

Fig. 1. The schematic of the experimental setup. (a) Two charge coupled device (CCD) cameras were used for optically tracking the markers glued to the facet joint capsule surface for subsequent strain calculations. (b) A human cadaveric lumbar spine specimen was fixed to the testing surface, with coordinate axes as shown. (c) A force transducer was used to measure the applied load. The loading apparatus consisted of (d) a displacement controlled linear actuator with (e) an optical position encoder for the determination of actuator position. (f) Biaxial inclinometers were attached to the facet joint capsule's respective anterior vertebral bodies for measurement of intervertebral angle.

Multichannel Filter; Krohn-Hite Corporation, Brockton, MA) using a cutoff frequency of 700 Hz and streamed to disk.

Plane strain calculations

Plane strains of a facet joint capsule were measured by optically tracking infrared markers (1.16 mm radius) fixed to the capsule surface. Markers were typically arranged in a 3×3 array, although occasionally for narrow capsules a 3×2 array was used. After calibration of the space volume, markers were imaged at 50 Hz using a commercially available kinematic system (Model 50; Qualisys, Inc., Glastonbury, CT), which consisted of two charge coupled device (CCD) cameras fitted with infrared light emitters and filters, appropriate lens, two video processors and software. The 3D coordinates of the resultant centroids were determined post hoc from the two-dimensional (2D) coordinates provided by each of the two video processors (resolution 10 μm in the x, y and z directions).

Capsular plane strains, relative to the vertical neutral position of the spine specimen, were calculated using an algorithm that was an extension of a 2D isoparametric finite element method (FEM) [15]. This algorithm accounted for the rotation of the plane (see Appendix 1), which typically occurred during the physiological spine motions. Each of the nine markers on a given capsule defined a node, from which four quadrilateral regions (or elements) were defined. Plane strains (ε_{xx}, ε_{yy} and ε_{xy}) were calculated for each node, and the strains for an element were calculated as the means of its respective four nodes.

Principal strains E1 and E2 (defined as the principal strains the directions of which were closest to the x-axis and y-axis, respectively) were calculated for each element using the mean element plane strains. Preliminary experiments indicated that for most of the capsular elements, the magnitudes of the principal strains (E1 and E2) typically had opposite signs (ie, one was positive, or tensile, and the other negative, or compressive, for a given motion). Thus, as has been done by others for cervical spine facet capsule strains [13], E1 and E2 were similarly organized as either "maximum" (positive) or "minimum" (negative) principal strains (hereafter denoted as $\hat{E}_1$ and $\hat{E}_2$, respectively) regardless of their respective absolute magnitudes.

Testing protocol

Each specimen was subjected to four motions: flexion, extension, left bending and right bending. For a given motion and facet joint, a trial consisted of 10 consecutive cycles to a given displacement of the spine specimen (10, 20, 30 and 40 mm of horizontal displacement of the T12 vertebra) at 10 mm/second. Because this study was designed to examine physiological motions, displacements were constrained to those producing joint moments at L5–S1 (location of the largest moment arm) less than 10 Nm, a threshold beyond which can produce load–displacement relationships suggestive of damage to soft tissues of the spine [18]. Specimens were tested by imaging one of the L5–S1 joint capsules during all motions, then the contralateral joint and repeating for the next cephalad joint. The intertrial recovery time was 3 minutes to allow sufficient time for the specimen to return to its normal physiological state, as estimated from previous studies on isolated cat knee joint capsule [8,19].

Data analysis and statistics

IVA was calculated as the difference between the angles measured at the vertebral bodies adjacent to the joint capsule of interest and was reported as the mean of 10 cycles at maximum displacements. Joint moments were calculated from the mean peak loads of the last 5 of the 10 cycles (when the load relaxation had reached equilibrium, Fig. 2) and moment arms (ie, distance from the applied load at T12 to the center of each facet joint). Principal strains at maximum displacements were reported as the means of the respective element strains of the 10 cycles in each trial.

For a given parameter (moment, IVA, principal strain) and motion type (flexion, extension, left and right bending), one-way analysis of variance (ANOVA) and post hoc Tukey tests were used to determine if the parameter differed significantly at a given joint level among the four displacement trials (SPSS SigmaStat [Chicago, IL], version 2.03; IL; $\alpha=0.05$). Similarly, the data collected for a given displacement were compared across joint levels. For each motion type, the relationship between a parameter and displacement was regressed. These relationships were compared among joint levels using a pairwise comparison of two linear regression lines (CLRL, $\alpha=0.05$) [20]. At each joint level, the IVA–moment relationship was compared pairwise using comparison of polynomial regression lines (CPRL, $\alpha=0.05$) [21].

Results

Of the seven lumbar spine specimens tested, one exhibited a 9-degree scoliosis, whereas the other six had scolioses less

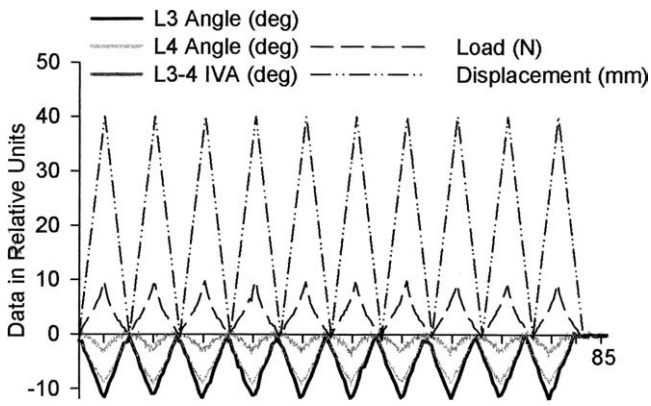

Fig. 2. Data for a representative trial, consisting of 10 cycles of flexion to 40 mm linear displacement (at T12). Load was measured at the point of application (at T12). The intervertebral angle (IVA) at L3–L4 was the difference between the rotations about the x-axis (Fig. 1) for L3 and L4.

than 5 degrees (as indicated by the X-rays of the specimens, obtained before dissection). No gross pathologies were evident by visual inspection or on plain film X-rays. Capsules were visually inspected at low-power magnification (×6) and were found to be intact, exhibiting characteristic gross normal appearance, including white color and a predominantly medial to lateral orientation of collagen fibrils [22].

Moment–displacement relationship

For the maximum displacements of the spine specimens (40 mm linear at T12), the joint moments were below the 10-Nm threshold (Fig. 3), and the largest average moment occurred during 40 mm of left bending (−5.33 Nm). For all motions, joint moment magnitudes significantly (ANOVA, $p<.001$) increased with increasing displacements, with the exception of L3–L4 during extension (Fig. 3). In trials where the difference in displacement was 20 mm or greater (eg, 10 mm vs 30 mm), a significantly greater moment was typically measured at the larger displacement (ANOVA, $p<.05$). The joint moments measured at a given motion and magnitude of displacement (with the exception of 40 mm right bending and left bending), were significantly larger in the more caudal facet joints (L4–L5 and L5–S1) than the cephalic joints (L1–L2 and L2–L3; ANOVA, $p<.05$).

The mean moment–displacement relationships for each joint were highly correlated (mean, $R^2=0.964$; range, 0.919 to 0.990). In all motion types, these relationships differed significantly among all joint levels; moments at a given joint level were significantly larger (ie, more positive in flexion, right bending, and more negative in extension, left bending) than those measured in the respective more cephalic joints (CLRL, $p<.05$).

Intervertebral angulation

During flexion and extension, the *x*-axis was the dominant axis of rotation for each of the vertebrae (Fig. 4, left), with the largest mean IVA measured at the L5–S1 joint for all displacements (greatest overall was 5.18 degrees, 40 mm of extension). In general, more positive angles were obtained with increasing displacements in extension, and more negative angles were measured with increasing displacements in flexion.

During extension, IVAs at a given joint level were significantly (ANOVA, $p<.02$) different from one another, although the trends varied at a given joint level (Fig. 4, left). At L1–L2, significantly different IVA were observed if the trials were separated by 30 mm displacement (ie, 40 mm vs 10 mm, $p=.01$). More caudal joints showed significant differences at smaller displacements, where significant trials were separated by 20 mm or greater displacement for both L4–L5 ($p<.03$) and L2–L3 ($p<.02$), and 10 mm or greater displacement for L5–S1 ($p<.03$); in all cases the angle measured at the larger displacement was greater. At a given displacement, the IVAs measured at L5–S1 were significantly larger than those measured at other joint levels ($p<.05$).

During flexion at a given joint level (Fig. 4, left), the IVA became larger for increasing displacements (ANOVA, $p<.05$); these differences were consistently significant for the caudal three motion units (L3–L4, L4–L5 and L5–S1; Tukey, $p<.005$). For a given displacement, significant differences were observed among IVAs across joint levels (ANOVA, $p<.001$); the angles measured at the more caudal joints (L4–L5 and L5–S1) were generally larger than those obtained at more cephalic joints (L1–L2, L2–L3 and L3–L4; Tukey, $p<.02$).

During left and right bending, the *z*-axis was the dominant axis of rotation (Fig. 4, right), with the largest angles obtained at the L3–L4 joint level for all displacements (largest mean IVA was 6.58 degrees, 40 mm left lateral bending). In general, angles became larger with increasing displacement (ie, more positive during left bending, more negative during right bending).

During left bending at a given joint level (Fig. 4, right), the IVAs were significantly different across displacement

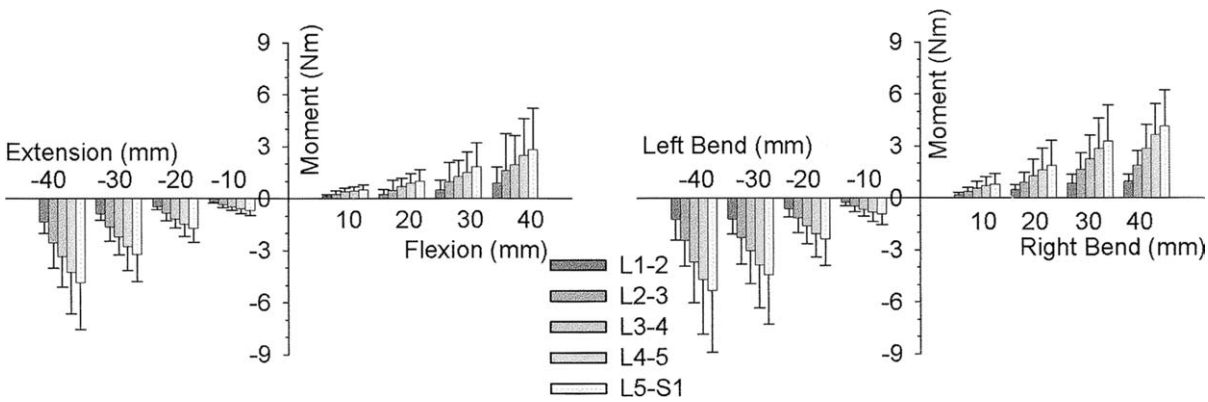

Fig. 3. Joint moments increased monotonically at a given joint level with increasing global displacements of the specimen during (left) extension and flexion, and (right) left and right lateral bending. At a given joint level, the mean moments were significantly larger (comparison of regression lines, $p<.05$) than those at the respective more cephalic joints. Error bars are standard deviations.

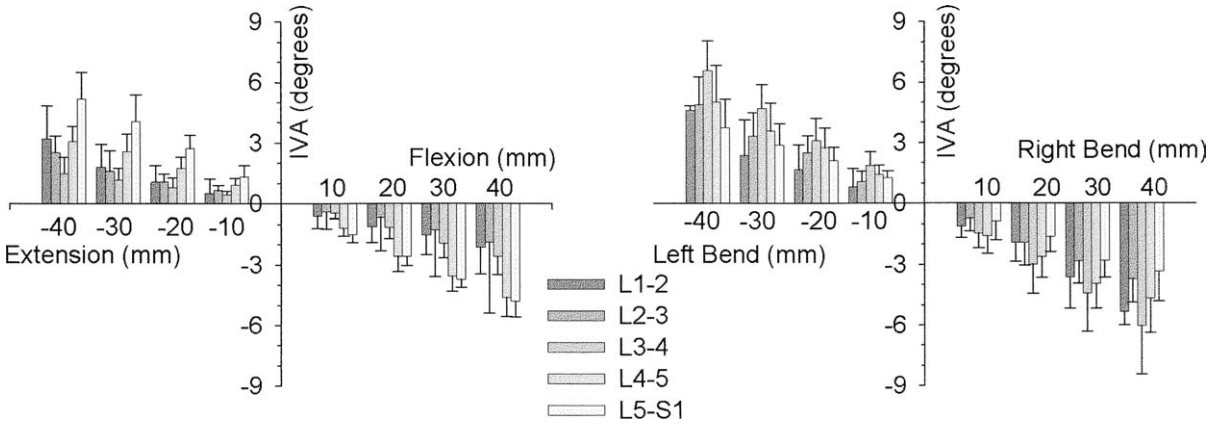

Fig. 4. Intervertebral angles (IVA) at a given joint level increased monotonically with increasing global displacements of the spine specimens. (Left) During extension and flexion, the IVA–displacement relationships at the more caudal vertebrae (L4–L5 and L5–S1) were significantly different compared with the more cephalic vertebrae (L1–L2, L2–L3 and L3–L4, comparison of regression lines, $p<.05$). (Right) During lateral bending, the IVA–displacement relationship at L3–L4 was significantly different compared with all other joints (comparison of regression lines, $p<.05$); at a given specimen displacement, larger IVAs occurred at L3–L4. Error bars show standard deviations.

(ANOVA, $p<.005$). IVA significantly increased at larger displacements at joint levels L2–L3, L3–L4 and L4–L5 (Tukey, $p<.05$). L1–L2 and L5–S1 exhibited similar trends, although these differences were not always significant. At a given displacement, significant differences were observed among the angles measured at each joint level (ANOVA, $p<.04$); the IVA obtained at L3–L4 for any given displacement was typically larger than those measured at L1–L2 and/or L5–S1 (Tukey, $p<.05$).

During right bending at a given joint level (Fig. 4, right), significant differences were observed among IVAs measured at different displacements (ANOVA, $p<.001$). Larger angles were measured at greater displacements if the difference between the displacements compared was greater than or equal to 20 mm (Tukey, $p<.05$). At a given displacement, there were significant differences among the IVAs measured across joint levels (ANOVA, $p<.05$), although there were no consistent trends or consistency in terms of which joint levels were different (Tukey, $p>.05$).

For each of the four motions, mean IVA–displacement relationships were highly correlated (mean, $R^2=0.984$; range, 0.927 to 1.0). The more caudal joints (L4–L5 and L5–S1) typically had significantly larger IVA than the more cephalic joints (L1–L2, L2–L3 and L3–L4) in both extension and flexion (CLRL, $p<.05$). In general, IVA measured during lateral bending at L3–L4 was significantly larger (CLRL, $p<.05$) than those measured at all other joint levels (with the exception of L4–L5 in right bending; CLRL $p>.05$). For each joint level, the mean IVA–moment relationship for extension–flexion was typically best fit using a regression of third-order polynomials (mean, $R^2=0.9856$; range, 0.975 to 0.999), and L1–L2 was the only joint level where this relationship was significantly different from the other motion units (CPRL, $p<.05$; Fig. 5, left). The mean IVA–moment relationships during lateral bending were typically best fit with second-order polynomials (mean, $R^2=0.978$; range, 0.945 to 0.991), although this relationship did not differ significantly among joint levels (CPRL, $p>.05$; Fig. 5, right).

Plane strains

For conciseness, only the two principal strains are reported; compared with ε_{xx}, ε_{yy} and ε_{xy}, they were typically largest in magnitude and, among the seven specimens, exhibited smaller variability. Data obtained from the right and left sides of the spines are reported separately, as they were significantly different (ANOVA, $p<.05$). Designating the principal strains as $\hat{E}_1$ and $\hat{E}_2$ was highly consistent with classification of the strains according to their directions (ie, E1 as closest to the *x*-axis and E2 as closest to the *y*-axis). During extension (where $\hat{E}_2$ was typically larger in absolute magnitude, although negative in sign), a larger percentage of $\hat{E}_2$ had their directions aligned closest to the *y*-axis (ie, were E2 82% on the left side of the spine, 75% on the right side of the spine). During flexion (where $\hat{E}_1$ was typically larger in absolute magnitude than $\hat{E}_2$), $\hat{E}_1$ was predominantly oriented closest to the *y*-axis (ie, were E2 83% on the left side of the spine and 77% on the right side of the spine). During left bending, 63% of $\hat{E}_1$ on the left side of the spine were oriented closest to the *x*-axis (ie, were E1) and 70% of $\hat{E}_1$ on the right side of the spine were oriented closest to the *y*-axis (ie, were E2). The opposite pattern was observed in trials of right bending, with E2 comprising 75% of $\hat{E}_1$ on the left side of the spine and E1 comprising 68% of $\hat{E}_1$ on the right side of the spine.

Intratrial strain data were highly repeatable in a pseudo-random selection of 40-mm trials encompassing all four motion types ($n=18$, average standard deviation of the peak strains and strain rates for 10 cycles were, respectively, 0.53% strain and 0.28% strain/second$\pm$1.2 SD with 95% confidence intervals of 5%). Regardless, with the relatively

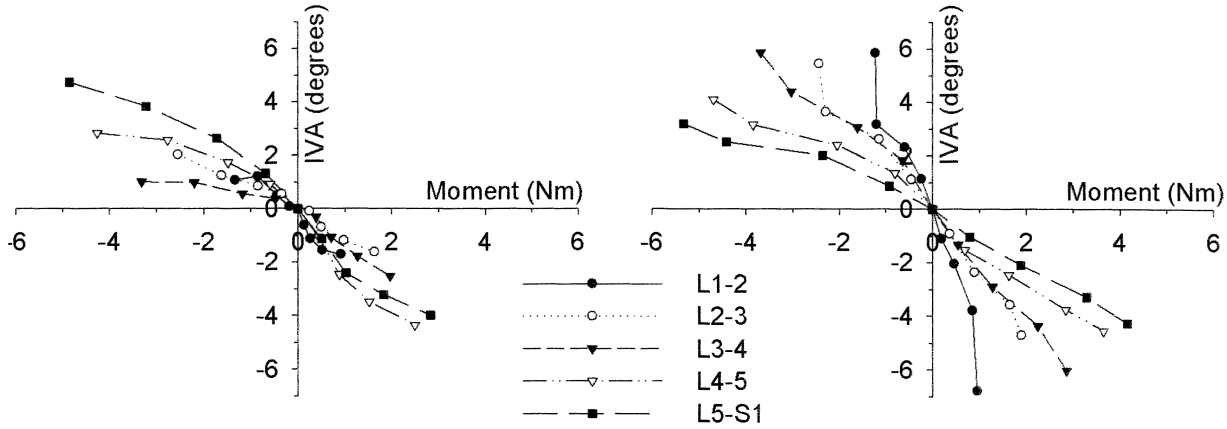

Fig. 5. Average intervertebral angle (IVA)–moment relationships were nonlinear. Although the moment is placed on the abscissa, for these experiments, displacement was the controlled parameter. (Left) Extension–flexion IVA–moment relationship. The largest extension moment (−4.8 Nm) occurred at L5–S1, which also exhibited the largest IVA (4.7 degrees). The largest flexion moment (2.8 Nm) also occurred at L5–S1, although the largest IVA (−4.4 degrees) occurred at L4–L5. (Right) Lateral bending IVA–moment relationship. All joints exhibited relative mirror symmetry during left bending (negative moments) and right bending (positive moments). IVA increased more substantially with increasing moments during lateral bending, especially in the more cephalic joints (L1–L2, L2–L3 and L3–L4). Error bars are not displayed here for clarity; refer to Figs. 3 (moment) and 4 (IVA) for *x* and *y* error bars, respectively.

large variability of regional capsule strains and the relatively small number of samples, ANOVA of the strain data fell short of the desired 80% power ($\hat{E}_1$ mean power 19.5%±23.7% SD, mode 5%; $\hat{E}_2$ mean power 25.3%±26.3%, mode 5%). The estimated sample size to achieve 80% power was 55 samples. Thus, comparisons of strain at a given displacement and/or joint level could not be analyzed for significance with a high degree of certainty. Because the linear regressions were not underpowered, only those results are reported.

In the vertical neutral position, the joint capsules appear to have been preloaded. Using visual observation during motions, no buckling of any of the capsules was ever observed. Because membranes in general do not support in-plane compression, it appears that the large negative principal strains observed, for example in extension, were the result of the capsule undergoing "relaxation" rather than in-plane compression per se. In general, the magnitudes of the strains increased with larger displacements (ie, $\hat{E}_1$ became more positive, $\hat{E}_2$ became more negative). Interspine mean regional principal strains were highly correlated with increasing displacements for all four motion types (mean R^2=0.86±0.23 SD, with only 22% of the trials having R^2<0.75). $\hat{E}_1$ was generally more highly correlated to displacement (mean R^2=0.86±0.23 SD, with only 18% of the $\hat{E}_1$ versus displacement relationships having R^2 less than 0.75) than was $\hat{E}_2$ (mean R^2=0.82±0.23, with approximately 28% of the $\hat{E}_2$ versus displacement relationships having R^2 less than 0.75).

Extension

In extension, mean $\hat{E}_2$ magnitude was largest in the L5–S1 capsule, decreased for more cephalic capsules and was smallest in the L1–L2 capsule (Fig. 6). The largest $\hat{E}_2$ occurred during 40-mm extension at the L5–S1 capsule (−11.0% strain). For increasing extension displacements, $\hat{E}_2$ strains (absolute magnitude) at the L5–S1 capsules were significantly larger compared with L1–L2 and L3–L4 capsules (CLRL, p<.05). The largest $\hat{E}_1$ occurred during 40 mm of extension at L2–L3 capsules (7.7% strain). Mean $\hat{E}_1$ strains at L5–S1 capsules were significantly greater than L1–L2 capsules (CLRL, p<.05).

Flexion

During flexion, $\hat{E}_2$ strains typically were significantly larger at the L4–L5 capsules than at L5–S1 (CLRL, p<.05). The largest $\hat{E}_2$ was measured during 40 mm of flexion at L3–L4 (−7.5% strain); at any given joint/displacement, $\hat{E}_2$ was generally smaller in absolute magnitude during flexion compared with extension. Typically during flexion, $\hat{E}_1$ magnitudes were largest in the most caudal capsules and decreased for more cephalic capsules (Fig. 6). At a given joint capsule, the absolute magnitude of $\hat{E}_1$ was larger than $\hat{E}_2$. Mean $\hat{E}_1$ strains in flexion were also larger than those during extension, and the largest mean $\hat{E}_1$ strain was during 40 mm flexion at the L4–L5 capsules (14.6% strain). Mean $\hat{E}_1$ strains at L1–L2 capsules were significantly smaller in magnitude than L4–L5 and L5–S1 capsules, and L2–L3 capsule strains were significantly smaller than L5–S1 capsule strains (CLRL, p<.05).

Lateral bending: left side

During lateral bending, on the left side of the spine, $\hat{E}_1$ strains of the capsules were typically larger in magnitude during right bending than during left bending (with the exception of L2–L3; Fig. 7, top). In right bending, L4–L5 $\hat{E}_1$ capsule strains were significantly larger than L1–L2 $\hat{E}_1$

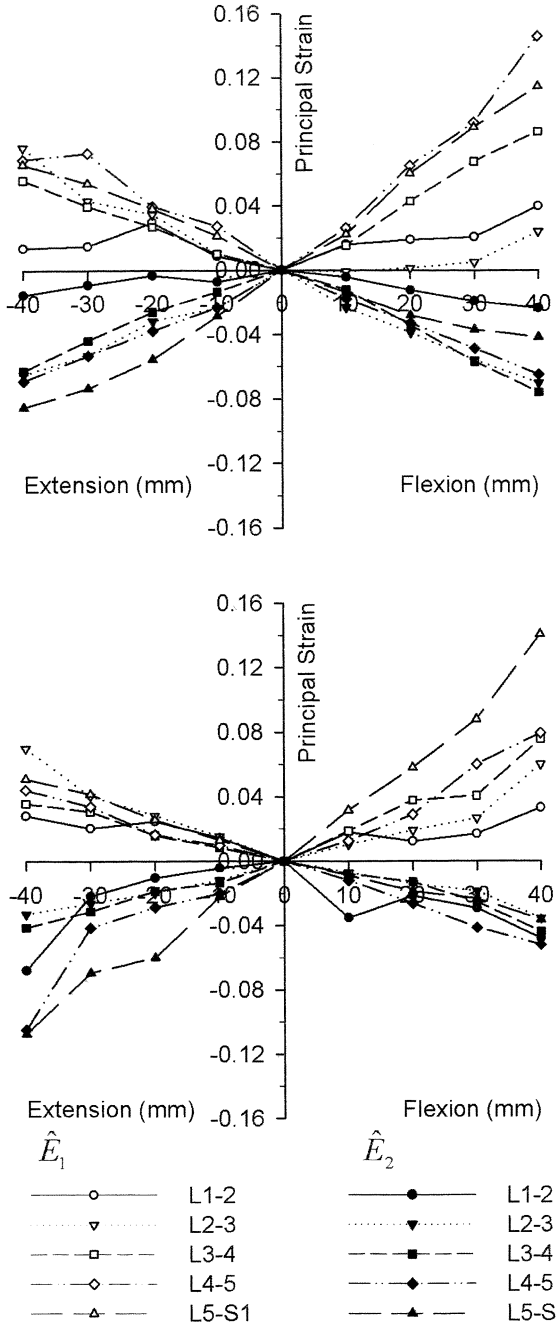

	Left Ext. $\hat{E}_2$ Std. Dev.					Left Ext. $\hat{E}_1$ Std. Dev.				
Displ (mm)	L1-2	L2-3	L3-4	L4-5	L5-S1	L1-2	L2-3	L3-4	L4-5	L5-S1
-40	0.01	0.03	0.01	0.01	0.02	0.01	0.06	0.05	0.06	0.04
-30	0.01	0.04	0.01	0.03	0.04	0.01	0.05	0.03	0.12	0.03
-20	0.01	0.06	0.02	0.04	0.05	0.05	0.03	0.02	0.05	0.02
-10	0.02	0.04	0.03	0.05	0.06	0.01	0.02	0.01	0.05	0.02
Ext. Sig.		*	*+	*	*		*	*	*	*
	Left Flex. $\hat{E}_2$ Std. Dev.					Left Flex. $\hat{E}_1$ Std. Dev.				
Displ (mm)	L1-2	L2-3	L3-4	L4-5	L5-S1	L1-2	L2-3	L3-4	L4-5	L5-S1
10	0.01	0.01	0.01	0.01	0.01	0.03	0.01	0.01	0.02	0.02
20	0.02	0.02	0.02	0.03	0.02	0.05	0.02	0.02	0.05	0.05
30	0.02	0.04	0.04	0.04	0.03	0.01	0.04	0.04	0.05	0.07
40	0.02	0.04	0.04	0.06	0.04	0.01	0.05	0.04	0.08	0.09
Flex. Sig.		*	*+	*+	*			*◦♦	*◦	*◦

	Right Ext. $\hat{E}_2$ Std. Dev.					Right Ext. $\hat{E}_1$ Std. Dev.				
Displ (mm)	L1-2	L2-3	L3-4	L4-5	L5-S1	L1-2	L2-3	L3-4	L4-5	L5-S1
-40	0.01	0.01	0.01	0.01	0.02	0.03	0.16	0.04	0.03	0.04
-30	0.02	0.02	0.01	0.02	0.03	0.03	0.05	0.03	0.03	0.03
-20	0.07	0.02	0.01	0.03	0.06	0.03	0.03	0.01	0.01	0.03
-10	0.15	0.03	0.01	0.21	0.06	0.02	0.02	0.01	0.01	0.01
Ext. Sig.			+	◦	*◦					*
	Right Flex. $\hat{E}_2$ Std. Dev.					Right Flex. $\hat{E}_1$ Std. Dev.				
Displ (mm)	L1-2	L2-3	L3-4	L4-5	L5-S1	L1-2	L2-3	L3-4	L4-5	L5-S1
10	0.02	0.01	0.01	0.01	0.01	0.01	0.01	0.03	0.02	0.03
20	0.03	0.02	0.03	0.02	0.02	0.02	0.01	0.08	0.03	0.06
30	0.04	0.03	0.04	0.03	0.03	0.02	0.03	0.17	0.05	0.07
40	0.05	0.05	0.07	0.04	0.04	0.04	0.08	0.03	0.07	0.09
Flex. Sig.				◦+				+	+	*+	*

Fig. 6. Maximum and minimum principal strains ($\hat{E}_1$ and $\hat{E}_2$, respectively; refer to text for definition) during extension (Ext) and flexion (Flex) on the (top) left and (bottom) right sides of the spine. At a given joint level, $\hat{E}_1$ was typically larger in absolute magnitude during flexion, whereas $\hat{E}_2$ was typically larger in absolute magnitude during extension. The inserted tables display standard deviations (Std Dev) for the mean strains at a given displacement (Displ) and indicate significant trends (Sig) among joint levels (comparison of regression lines, $p<.05$; the symbols *, ○, ♦, and + indicate significant differences from L1–L2, L2–L3, L4–L5 and L5–S1, respectively).

capsule strains (CLRL, $p<.05$). L2–L3 $\hat{E}_1$ capsule strains were significantly smaller than all other joint levels (CLRL, $p<.05$). There were fewer consistent trends in $\hat{E}_1$ during left bending. Overall, the largest $\hat{E}_1$ strains were measured at the L4–L5 capsules during 40 mm of right bending (8.6% strain).

$\hat{E}_2$ strains on the left side of the spine during lateral bending were typically larger in right bending than during left bending, with the exception of L5–S1 capsules. During right bending, the left L5–S1 capsule $\hat{E}_2$ strains were significantly (CLRL, $p<.05$) smaller in absolute magnitude than the three more cephalic joint capsules (L1–L2, L2–L3 and L3–L4); there were no significant differences in $\hat{E}_2$ among the joint capsules during left bending. The largest $\hat{E}_2$ capsular strains on the left side occurred at L2–L3 during 40 mm of right bending (−7.9% strain).

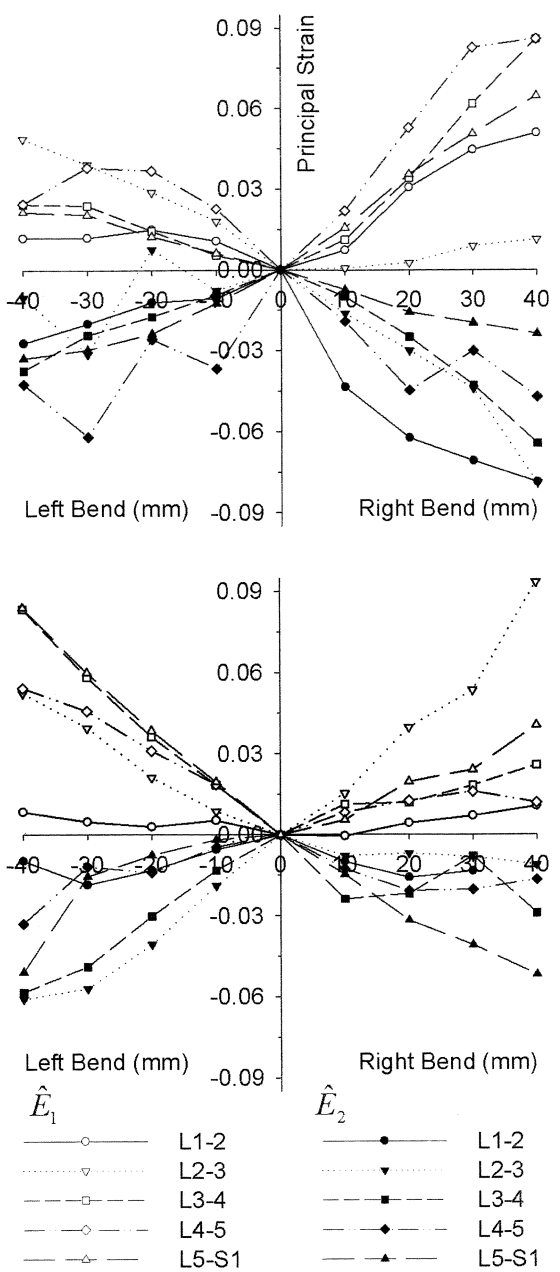

	Left LB $\hat{E}_2$ Std. Dev.					Left LB $\hat{E}_1$ Std. Dev.				
Displ (mm)	L1-2	L2-3	L3-4	L4-5	L5-S1	L1-2	L2-3	L3-4	L4-5	L5-S1
-40	0.01	0.03	0.01	0.06	0.01	0.02	0.07	0.05	0.02	0.02
-30	0.04	0.02	0.02	0.02	0.02	0.02	0.05	0.03	0.10	0.02
-20	0.02	0.06	0.02	0.12	0.02	0.02	0.03	0.02	0.08	0.01
-10	0.04	0.04	0.02	0.03	0.03	0.01	0.02	0.01	0.05	0.01
LB Sig.							*			○
	Left RB $\hat{E}_2$ Std. Dev.					Left RB $\hat{E}_1$ Std. Dev.				
Displ (mm)	L1-2	L2-3	L3-4	L4-5	L5-S1	L1-2	L2-3	L3-4	L4-5	L5-S1
10	0.06	0.02	0.01	0.02	0.01	0.01	0.02	0.01	0.02	0.02
20	0.08	0.04	0.02	0.10	0.02	0.04	0.03	0.03	0.04	0.04
30	0.10	0.05	0.03	0.03	0.03	0.06	0.05	0.06	0.07	0.05
40	0.12	0.05	0.05	0.04	0.04	0.06	0.08	0.06	0.06	0.08
RB Sig	+	+	+				*	○	○ *	○

	Right LB $\hat{E}_2$ Std. Dev.					Right LB $\hat{E}_1$ Std. Dev.				
Displ (mm)	L1-2	L2-3	L3-4	L4-5	L5-S1	L1-2	L2-3	L3-4	L4-5	L5-S1
-40	0.01	0.02	0.01	0.01	0.01	0.01	0.04	0.07	0.05	0.07
-30	0.01	0.04	0.03	0.02	0.01	0.01	0.03	0.06	0.04	0.05
-20	0.03	0.05	0.04	0.04	0.01	0.01	0.02	0.04	0.03	0.03
-10	0.00	0.06	0.07	0.03	0.04	0.01	0.01	0.02	0.02	0.01
LB Sig.		*	♦	○	* ○		*	* +		
	Right RB $\hat{E}_2$ Std. Dev.					Right RB $\hat{E}_1$ Std. Dev.				
Displ (mm)	L1-2	L2-3	L3-4	L4-5	L5-S1	L1-2	L2-3	L3-4	L4-5	L5-S1
10	0.00	0.02	0.02	0.01	0.01	0.01	0.02	0.02	0.01	0.01
20	0.02	0.03	0.03	0.02	0.02	0.01	0.04	0.02	0.01	0.02
30	0.01	0.04	0.07	0.02	0.03	0.01	0.06	0.03	0.02	0.02
40	-	0.07	0.03	0.02	0.02	0.01	0.11	0.03	0.01	0.03
RB Sig		+	+	+			*	*	○ +	*

Fig. 7. Maximum and minimum principal strains ($\hat{E}_1$ and $\hat{E}_2$, respectively; refer to text for definition) during left bending (LB) and right bending (RB) on the (top) left and (bottom) right sides of the spine. At a given joint level, $\hat{E}_1$ was typically larger in absolute magnitude during tensile motions, whereas $\hat{E}_2$ was typically larger in absolute magnitude during compressive motions. The inserted tables display standard deviations (Std Dev) for the mean strains at a given displacement (Displ) and indicate significant trends (Sig) among joint levels (comparison of regression lines, $p < .05$; the symbols *, ○, ♦, and + indicate significant differences from L1–L2, L2–L3, L3–L4, L4–L5 and L5–S1, respectively).

Lateral bending: right side

On the right side of the spine, $\hat{E}_1$ strains of the joint capsules during left bending were typically larger in magnitude in the more caudal joints (L3–L4, L4–L5, L5–S1) than those measured during right bending, whereas the opposite was true for the more cephalic joint capsules (L1–L2 and L2–L3; Fig. 7). During right bending, $\hat{E}_1$ at the L1–L2 capsules was significantly smaller in magnitude compared with the caudal capsules (L2–L3, L3–L4 and L5–S1); L4–L5 $\hat{E}_1$ capsule strains were significantly smaller than those in the L2–L3 and L5–S1 capsules (CLRL, $p<.05$). During left bending, $\hat{E}_1$ strains of the L1–L2 capsule were significantly smaller than those in L2–L3 and L3–L4 capsules, and the L3–L4 capsule strains were significantly smaller in magnitude than those in the L5–S1 capsule (CLRL, $p<.05$). The largest $\hat{E}_1$ capsular strains were measured during 40 mm of right bending at the L2–L3 joint (9.4% strain).

During left bending, $\hat{E}_2$ strains were generally larger in the more cephalic joint capsules (L1–L2, L2–L3 and L3–L4) compared with the more caudal joint capsules (L4–L5

and L5–S1); the opposite was true during right bending. In left bending, $\hat{E}_2$ strains at L1–L2 capsules differed significantly from those in the L2–L3 and L5–S1 capsules (CLRL, $p<.05$). L2–L3 capsular strains were significantly larger than the L4–L5 and L5–S1 capsules, and L3–L4 capsular strains were significantly larger than L4–L5 capsules (CLRL, $p<.05$ for all). During right bending, $\hat{E}_2$ at L5–S1 capsules was significantly larger than all other joint capsules (CLRL, $p<.05$). The largest $\hat{E}_2$ strain (absolute value) was measured at L2–L3 capsules during 40 mm of left bending (−6.1% strain).

In general, at a given joint level, the motion (flexion/extension vs left bending/right bending) during which the joint experienced the largest IVA was the same motion during which the largest principal strain occurred (Table 1). In addition, if a comparison between the IVA-displacement regressions for two joints was statistically significant, then it was likely that a significant comparison of the same joints was observed in the principal strain-displacement regressions (particularly during motions producing strains of high magnitude, as in flexion).

Discussion

To our knowledge, this is the first report of in situ plane strains in lumbar facet joint capsules developed during physiological motions of ligamentous lumbar spine specimens (T12 sacrum). From full extension to full flexion of the lumbar spine, mean principal strains of the joint capsules increased monotonically with the largest strains occurring in the most caudal joint capsules. Capsule strains during left and right bending demonstrated relative mirror symmetry. These data provide support for the concept that joint capsule loading could provide a biomechanical signal for lumbar spine proprioception.

Using a displacement-controlled apparatus, the IVAs in the current study were similar to those obtained by Panjabi et al. [23] using a moment-controlled apparatus. In both studies, the maximum IVAs during flexion and extension trials were measured at L5–S1 and averaged approximately 5 degrees (compare Fig. 4, left, in current study with Fig. 3 in Panjabi et al. [23]). In the current study, the maximum IVA during lateral bending was at L3–L4 (6.6 degrees), whereas in Panjabi et al. [23] the maximum IVA was at L2–3 (5.3 degrees) (compare Fig. 4, right, in current study with Fig. 5 in Panjabi et al. [23]); however, in both cases these values were not significantly different from IVA measured at other joints. Indeed, the IVA for a given moment appears to be similar in both studies (ie, the mean IVAs in this study typically appeared within their respective standard deviations).

Table 1
Motions creating the largest intervertebral angle and principal strain for each joint level

Joint level	Maximum IVA (degrees)	Largest strain
L1–L2	RB (−6.77)	RB (0.050)
L2–L3	LB (5.44)	RB (0.090)
L3–L4	RB (−6.0)	RB (0.086)
L4–L5	F (−4.54)	F (0.146)
L5–S1	E (5.18)	F (0.140)

E=extension; F=flexion; IVA=intervertebral angle; LB=left bending; RB=right bending.

Despite high variability within the data, consistent patterns of strain related to specimen position were observed. Although intracapsular strains were heterogeneous, similar to those observed in the cervical spine [13], elemental strains systematically increased with increasing displacements of flexion/extension. For a given lumbar facet joint capsule, the motion during which the joint displaced the most (ie, a maximum IVA was measured) was the same type of motion during which the capsular ligament experienced the largest strains. When considering the lumbar spine as a whole, significant differences in the IVA–displacement relationships for motion segments usually meant that their strain–displacement relationships were significantly different as well. This was most strongly observed during flexion and less so during motions of extension, left and right bending, possibly because of differences in the mechanics of each motion. These trends were in contrast to the lack of consistent strain patterns observed in cervical spine facet joint capsules [13], which may be the result of the anatomical differences between the cervical and lumbar spines.

Lumbar facet capsule principal strains (tensile) in the current study were similar in magnitude to uniaxial facet capsule strains reported by Panjabi et al. [14], although the joint moments in the current study were much smaller. An explanation for this was the relative sigmoidal relationship between intervertebral angles and joint moment, as shown in the current study as well as by Panjabi et al. [23] and in cervical spine in vivo [24]. For larger moments, the IVAs plateau, and there was minimal increase in IVA with increasing moment [23]. The current study depicted similar nonlinear relationships (Fig. 5), although because the developed moments were smaller, there was less demonstration of a plateau. Because the facet joint capsule strains were related to the IVAs, then with similar IVAs in both studies it was reasonable that they would have comparable magnitudes of capsule strains.

Similar to observations in the cervical spine [13], the lumbar facet joint capsules often experience both in-plane tensile and compressive strains simultaneously in response to physiological motions (ie, in over 80% of the trials in the current study). Hence, when reporting plane principal strains in facet capsule, it was valuable to present both principal strains. For example, in lumbar facet capsules the maximum principal strains ($\hat{E}_1$ in the current study) were typically larger (more positive) during tensile motions (ie, flexion and lateral bending contralateral to the facet joint of interest) than in compressive motions (ie, extension and lateral bending toward the facet joint of interest); the opposite was generally

observed when considering the minimum principal strains ($\hat{E}_2$ in the current study), particularly during extension and flexion. For this reason, significant relationships or trends between motions and capsule strains were generally not apparent in $\hat{E}_1$ strains during compressive motions, whereas several trends were identified in $\hat{E}_2$ strains for the same motions. Thus, although presenting both principal strains was more complex, some significant relationships became apparent that might have otherwise been missed.

The organization of the principal strains as maximum ($\hat{E}_1$) and minimum ($\hat{E}_2$) was supported by the fact that a large percentage of the strains in either group had the same orientation (ie, were either E1 or E2). In addition, the dominant orientation of the principal strain largest in magnitude was logical when considering motion type and capsule location. For instance, during compressive motions one would expect that the capsule would compress along the *y*-axis and thus elongate along the *x*-axis. Conversely, during tensile motions, one would expect that the capsule would elongate along the *y*-axis and compress along the *x*-axis. The data were generally consistent with this reasoning for all four motion types.

There are a number of constraints that should be considered when interpreting the results from the current study. First, the specimens were obtained from older adults, and preliminary data (not shown) from our laboratory for younger spines, which generally are much more flexible, suggest that capsule strains in younger spines can be much larger for the same joint moment. Second, the variability in the data was relatively high, which was likely the result of a combination of factors, including age, gender and relative overall health of the donors. Furthermore, the variability in strain patterns may have been exaggerated by differences in marker placement, because in some cases it was necessary to place the array of markers in an irregular pattern or to use fewer markers because of capsule morphology. Although an irregularly shaped element would not have affected the accuracy of the strain measurement, a difference in marker placement could affect principal strain patterns from one capsule to the next (given the heterogeneity of strains on the capsular surface). Variability was also no doubt influenced by slight differences in collagen fiber orientation in different regions of the capsular surface and/or multiple points of insertion of the capsular ligament [22]. Orienting the spine in its neutral position using visual inspection alone may have increased the variability observed among the spine specimens as opposed to using other inspection techniques. However, these increases are likely to be small, as X-ray validation of the neutral position was shown to result in similar IVA variability [23]. Finally, in spite of precautions to keep the spine specimens moist, each capsule was exposed directly to air for significant periods of time, and each of the spine specimens underwent a few freeze-thaw cycles, all of which could have affected the measured strains.

It is well established that facet joint capsules are innervated with mechanoreceptors and nociceptors [1,6,10,11,25,26], and it follows that this system may serve proprioceptive functions [4,27]. It has been demonstrated in animal models that afferents innervating the lumbar facet capsule and surrounding tissue respond to capsular manipulation [10] and stretch [11]. The current study provides biomechanical evidence that there is a consistent pattern of facet capsule strains associated with lumbar motions, and thus provides support to this proprioceptive theory in human lumbar spines.

Appendix

Calculation of plane strains during plane rotation

To account for capsule plane rotation, four general modifications were necessary and made to the 2D isoparametric finite element method of Hoffman and Grigg [15] for calculating plane strains. First, all marker centroids were measured in 3D (*x*, *y*, *z*), rather than 2D (*x*, *y*). Second, isoparametric "brick" (eight-noded) elements were created rather than 2D quadrilateral (four-noded) planar elements. These brick elements consisted of the four "real" nodes defined from the measured centroids of four markers, and four "virtual" nodes, each of which was normal to the actual plane and respectively projecting from a real node at a constant arbitrary, but reasonable, distance of 1 mm (Fig. A1). Hence, brick elements of constant 1-mm thickness were created. Third, Lagrangian strains were calculated using a full 3D approach for each of the eight nodes of a brick element. The "real" quadrilateral and its virtual nodes were then mapped from Cartesian (*x*, *y*, *z*) to natural (*s*, *t*, *r*) coordinates using interpolation functions [28] (equations A1 to A8).

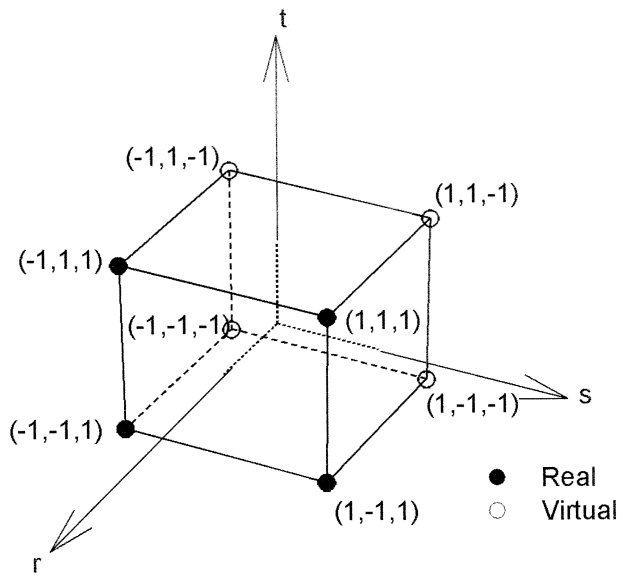

Fig. A1. Eight-noded "brick" element, created by the four front real nodes (ie, centroids of the markers fixed to the facet joint capsule surface) and the four virtual nodes, for plane strain calculations using a three-dimensional finite element method. Natural coordinate axes (*r*, *s*, *t*) are shown.

$$N_1 = \frac{1}{8}(1-s)(1-t)(1+r) \quad \text{(A1)}$$

$$N_2 = \frac{1}{8}(1+s)(1-t)(1+r) \quad \text{(A2)}$$

$$N_3 = \frac{1}{8}(1+s)(1+t)(1+r) \quad \text{(A3)}$$

$$N_4 = \frac{1}{8}(1-s)(1+t)(1+r) \quad \text{(A4)}$$

$$N_5 = \frac{1}{8}(1-s)(1-t)(1-r) \quad \text{(A5)}$$

$$N_6 = \frac{1}{8}(1+s)(1-t)(1-r) \quad \text{(A6)}$$

$$N_7 = \frac{1}{8}(1+s)(1+t)(1-r) \quad \text{(A7)}$$

$$N_8 = \frac{1}{8}(1-s)(1+t)(1-r) \quad \text{(A8)}$$

As was done in Hoffman and Grigg [15], these interpolation functions were used in calculating the spatial partial derivatives of the nodal initial positions (x, y, z) and displacements (u, v, w) (hence, this approach was an isoparametric finite element method). The chain rule then yields the partial derivatives expressions of the nodal displacements in the natural coordinate system for the 3D isoparametric element (equations A9 to A11).

$$\begin{Bmatrix} \frac{\partial u}{\partial s} \\ \frac{\partial u}{\partial t} \\ \frac{\partial u}{\partial r} \end{Bmatrix} = \begin{pmatrix} \frac{\partial x}{\partial s} & \frac{\partial y}{\partial s} & \frac{\partial z}{\partial s} \\ \frac{\partial x}{\partial t} & \frac{\partial y}{\partial t} & \frac{\partial z}{\partial t} \\ \frac{\partial x}{\partial r} & \frac{\partial y}{\partial r} & \frac{\partial z}{\partial r} \end{pmatrix} \begin{Bmatrix} \frac{\partial u}{\partial x} \\ \frac{\partial u}{\partial y} \\ \frac{\partial u}{\partial z} \end{Bmatrix} \quad \text{(A9)}$$

$$\begin{Bmatrix} \frac{\partial v}{\partial s} \\ \frac{\partial v}{\partial t} \\ \frac{\partial v}{\partial r} \end{Bmatrix} = \begin{pmatrix} \frac{\partial x}{\partial s} & \frac{\partial y}{\partial s} & \frac{\partial z}{\partial s} \\ \frac{\partial x}{\partial t} & \frac{\partial y}{\partial t} & \frac{\partial z}{\partial t} \\ \frac{\partial x}{\partial r} & \frac{\partial y}{\partial r} & \frac{\partial z}{\partial r} \end{pmatrix} \begin{Bmatrix} \frac{\partial v}{\partial x} \\ \frac{\partial v}{\partial y} \\ \frac{\partial v}{\partial z} \end{Bmatrix} \quad \text{(A10)}$$

$$\begin{Bmatrix} \frac{\partial w}{\partial s} \\ \frac{\partial w}{\partial t} \\ \frac{\partial w}{\partial r} \end{Bmatrix} = \begin{pmatrix} \frac{\partial x}{\partial s} & \frac{\partial y}{\partial s} & \frac{\partial z}{\partial s} \\ \frac{\partial x}{\partial t} & \frac{\partial y}{\partial t} & \frac{\partial z}{\partial t} \\ \frac{\partial x}{\partial r} & \frac{\partial y}{\partial r} & \frac{\partial z}{\partial r} \end{pmatrix} \begin{Bmatrix} \frac{\partial w}{\partial x} \\ \frac{\partial w}{\partial y} \\ \frac{\partial w}{\partial z} \end{Bmatrix} \quad \text{(A11)}$$

Solving for the right-most vectors in equations A9 to A11 then allows for plane strain calculations using the Lagrangian large strain formulation [29].

Fourth, strain artifacts resulting from plane rotation were eliminated by performing a coordinate transformation of the 3D strains relative to the original reference plane (ie, where the spine was in its neutral or reference position). The transformation matrix [T] was determined by the matrix operation necessary to transform the plane of the deformed nodes [n] such that it would be parallel to the reference plane [n'] [30]:

$$n' = [\mathrm{T}]n \quad \text{(A12)}$$

Then, the nodal strain tensor was multiplied by this transformation matrix:

$$E' = [\mathrm{T}]E \quad \text{(A13)}$$

Because the thickness was held constant, all out-of-plane shears became identically zero (ie, $\varepsilon_{yz}=\varepsilon_{xz}=\varepsilon_{zy}=\varepsilon_{zx}=0$) from the transformation, resulting in plane strains from a 3D strain calculation method.

Validation of this algorithm was performed as follows: 1) 3D coordinates of four reference nodes and their coordinates following known, arbitrary deformations, but without plane rotation, were input, and the algorithm correctly calculated the respective plane strains; 2) 3D coordinates of quadrilaterals at arbitrary planes of rotations, but without any internodal displacement, were input. This correctly resulted in zero strain; 3) nodal coordinates of known displacements and plane rotations were input, which resulted in correct calculation of plane strains.

References

[1] Cavanaugh JM, Ozaktay AC, Yamashita T, Avramov A, Getchell TV, King AI. Mechanisms of low back pain: a neurophysiologic and neuroanatomic study. Clin Orthop 1997;1:166–80.

[2] Yang KH, King AI. Mechanism of facet load transmission as a hypothesis for low-back pain. Spine 1984;9:557–65.

[3] Helbig T, Lee CK. The lumbar facet syndrome. Spine 1988;13:61–4.

[4] Pickar JG. Neurophysiological effects of spinal manipulation. Spine J 2002;2:357–71.

[5] Cavanaugh JM, Ozaktay AC, Yamashita HT, King AI. Lumbar facet pain: biomechanics, neuroanatomy, and neurophysiology. J Biomech 1996;29:1117–29.

[6] McLain RF, Pickar JG. Mechanoreceptor endings in human thoracic and lumbar facet joints. Spine 1998;23:168–73.

[7] Grigg P. Properties of sensory neurons innervating synovial joints. Cells Tissues Organs 2001;169:225.

[8] Khalsa PS, Hoffman AH, Grigg P. Mechanical states encoded by stretch-sensitive neurons in feline joint capsule. J.Neurophysiol 1996;76:175–87.

[9] Sjolander P, Johansson H, Djupsjobacka M. Spinal and supraspinal effects of activity in ligament afferents. J Electromyogr Kinesiol 2002;12:167–76.

[10] Pickar JG, McLain RF. Responses of mechanosensitive afferents to manipulation of the lumbar facet in the cat. Spine 1995;20:2379–85.

[11] Avramov A, Cavanaugh JM, Ozaktay AC, Getchell TV, King AI. The effects of controlled mechanical loading on group-II, III, and IV afferent units from the lumbar facet joint and surrounding tissue: an in vitro study. J Bone Joint Surg 1992;74A:1464–71.

[12] El-Bohy AA, Goldberg SJ, King AI. Measurement of facet capsular stretch. 1987 Biomechanics Symposium. Paper presented at: 1987 American Society of Mechanical Engineers Applied Mechanics, Bioengineering, and Fluids Engineering Conference, June 14–17, 1987, New York, NY. p. 161–4.

[13] Winkelstein BA, Nightingale RW, Richardson WJ, Myers BS. The cervical facet capsule and its role in whiplash injury: a biomechanical investigation. Spine 2000;25:1238–46.

[14] Panjabi MM, Goel VK, Takata K. Physiologic strains in the lumbar spinal ligaments. An in vitro biomechanical study. 1981 Volvo Award in Biomechanics. Spine 1982;7:192–203.

[15] Hoffman AH, Grigg P. A method for measuring strains in soft tissue. J Biomech 1984;17:795–800.

[16] Chiu J. Facet joint capsule strains of human lumbar spine specimens during physiological motions. 2001 Master's Thesis. State University of New York at Stony Brook.

[17] Saldanha A, Kawchuk G, Tateosian V, Khalsa PS. Control software for measuring physiological, dynamic facet capsule strains in human, lumbar spine specimens. Landover, MD: Biomedical Engineering Society, 2000:14671.

[18] Panjabi MM, Krag M, Summers D, Videman T. Biomechanical time-tolerance of fresh cadaveric human spine specimens. J Orthop Res 1985;3:292–300.

[19] Khalsa PS, Grigg P. Responses of mechanoreceptor neurons in the cat knee joint capsule before and after anterior cruciate ligament transection. J Orthop Res 1996;14:114–22.

[20] Glantz SA. How to test for trends: primer of biostatistics. 4th ed. New York: McGraw-Hill, 1997;238–41.

[21] Glantz SA, Slinker BK. Regression with two or more independent variables: primer of applied regression and analysis of variance. 2nd ed. New York: McGraw-Hill, 2001;54–107.

[22] Yamashita T, Minaki Y, Ozaktay AC, Cavanaugh JM, King AI. A morphological study of the fibrous capsule of the human lumbar facet joint. Spine 1996;21:538–43.

[23] Panjabi MM, Oxland TR, Yamamoto I, Crisco JJ. Mechanical behavior of the human lumbar and lumbosacral spine as shown by three-dimensional load-displacement curves. J Bone Joint Surg Am 1994; 76:413–24.

[24] McClure P, Siegler S, Nobilini R. Three-dimensional flexibility characteristics of the human cervical spine in vivo. Spine 1998;23:216–23.

[25] Yamashita T, Cavanaugh JM, El-Bohy AA, Getchell TV, King AI. Mechanosensitive afferent units in the lumbar facet joint. J.Bone Joint Surg [Am] 1990;72:865–70.

[26] McLain RF. Mechanoreceptor endings in human cervical facet joints. Spine 1994;19:495–501.

[27] Pickar JG. An in vivo preparation for investigating neural responses to controlled loading of a lumbar vertebra in the anesthetized cat. J Neurosci Methods 1999;89:87–96.

[28] Grandin H. Fundamentals of the finite element method. Prospect Heights, IL: Waveland Press, 1991.

[29] Malvern LE. Finite strain and deformation: introduction to the mechanics of a continuous medium. London: Prentice-Hall International, 1969:154–72.

[30] Chung TJ. Vectors and tensors: applied continuum mechanics. Cambridge: Cambridge University Press, 1996:4–15.